Bulletin of Earthquake Engineering (2021) 19:1537–1567
https://doi.org/10.1007/s10518-020-01038-0

ORIGINAL ARTICLE

A novel all-steel buckling restrained brace for seismic drift mitigation of steel frames

Nader Hoveidae[1] · **Saeed Radpour**[1]

Received: 7 July 2020 / Accepted: 29 December 2020 / Published online: 12 January 2021
© The Author(s), under exclusive licence to Springer Nature B.V. part of Springer Nature 2021

Abstract
Buckling restrained braces (BRBs) as metallic dampers can supply stable and balanced hysteretic response. While BRBs exhibit outstanding energy dissipation capacity, their low post-yield stiffness contributes to large residual drift concentration in simply supported buckling restrained braced frames. The present study introduces a novel all-steel tube-in-tube BRB composed of a short-length hybrid core serially connected to a non-yielding robust member. The hybrid core includes short-length yielding members made up of circular hollow sections surrounded by an all-steel encasing system. High strain hardening capacity of short-length hybrid core enhances the post-yield stiffness, thus reducing the residual drift in simply supported buckling restrained braced frame. In this paper, first the components of proposed brace are represented in detail. Subsequently, the design procedure and stability analysis results are provided. The feasibility of conceptual hybrid BRB is evaluated by finite element analysis method. Afterwards, the global response of prototype buckling restrained braced frames comprising conventional and proposed braces are appraised via pushover and nonlinear time history analyses. The analyses results designated the significant efficiency of proposed braces to help mitigate inter-story and particularly residual drifts in buckling restrained braced frames.

Keywords Short-length hybrid core · Buckling restrained brace · Stability analysis · Finite element analysis · pushover analysis · Time history analysis · Residual drift

1 Introduction

Buckling restrained braces are broadly employed as structural ductile fuse members. BRBs are gaining increasing favor by the engineers and fabricators, owing to their excellent ductility and seismic energy dissipation capacity. Commonly, axially decoupled restrainers are utilized to inhibit global buckling of BRBs and minimize the core high-mode buckling amplitudes. Regardless of exceptional ductility and energy dissipation

✉ Nader Hoveidae
Hoveidaei@azaruniv.ac.ir

Saeed Radpour
S.Radpour@azaruniv.ac.ir

[1] Civil Engineering Department, Azarbaijan Shahid Madani University, Tabriz, Iran

capacity of BRBs, one of the major challenging issues in design of typical simply supported buckling restrained braced frames (BRBFs) is their low post-yield stiffness and thus relatively large residual drifts.

During past decades, a number of experimental and theoretical studies have focused on seismic response of BRBs (Sabelli et al. 2003; Fahnestock et al. 2003; Watanabe et al. 1988; Hoveidae and Rafezy 2012), and have proposed unified design methods for conventional buckling restrained braces (Fahnestock et al. 2007; Kersting et al. 2015). Recently, significant attention has been paid to a new generation of unbonded brace called all-steel BRB, which is entirely made up of steel components (Tremblay et al. 2006; Della Corte et al. 2014; Piedrafita et al. 2015). Most of investigations on BRBs concentrate on seismic performance evaluation. Several recent studies have confirmed that BRBFs are susceptible to relatively large residual drifts. Macrae et al. (2004) found that low post-yield stiffness of BRBFs decreases their capability to distribute inter-story drifts along the height of structure. In addition, Zaruma and Fahnestock (2018) studied the seismic performance of buckling restrained braced frames and it was concluded that the low post-yield stiffness amplifies the residual drift demands and raises the collapse probability of buckling restrained braced frames under severe seismic events. Several solutions have been addressed to diminish residual drifts in BRBFs, comprising dual buckling restrained braced frames (Wada et al. 1992), short-length buckling restrained braces (Hoveidae et al. 2015; Pandikkadavath and Sahoo 2016), self-centering BRBs (Wang et al. 2017; Qin et al. 2020), and BRBs equipped with dampers (Yamamoto and Sone 2014). However, some of these techniques necessitate significant costs or extra structural modules. A novel BRB with reduced-length core for residual drift reduction of simply supported buckling restrained braces was recently proposed by Hoveidae et al. (2015), and it was resulted that the proposed BRB significantly decreased the permanent drifts in the braced frame. Global buckling behavior of reduced-length BRBs was investigated by Tong et al. (2020). Ghowsi and Sahoo (2018) numerically studied the seismic performance of hybrid self-centering buckling restrained braced frames. The analysis results showed superior seismic performance of hybrid system compared with ordinary buckling restrained braced frame. Finite element analysis of BRBs using full-scale experimental data was conducted by Avci-Karatas et al. (2019), and a convergence analysis regarding element numbers in the developed model was conducted for each BRB specimen. Finally, key issues that influenced the hysteretic modeling of BRBs were identified. Moreover, Hosseinzadeh and Mohebbi (2016) investigated the seismic response of all-steel BRBs using finite element analysis in ABAQUS. It was resulted that the inter-story drifts under near-fault records were higher compared with far-field records. In addition, the response modification factor R in BRBFs was around 50% larger than that of the X-braced frames. Experimental and numerical studies of reduced-length BRBs were conducted by Razavi et al. (2014), and the test results showed suitable performance of the specimens. Furthermore, the proposed stopper and debonding mechanism worked successfully.

Reducing the core length increases the elastic stiffness of the brace, which limits the lateral story drifts in weak to moderate earthquakes (Hoveidae et al. 2015; Pandikkadavath and Sahoo 2016). A short-length BRB is classically stiffer than a full-length conventional buckling restrained brace. As a result, the braced frames equipped with short-length BRBs are expected to absorb higher seismic forces. However, while the empirical period that is dependent on structural height governs the design, the application of short-length BRBs would not change the seismic input, in comparison to conventional BRBs.

The strain hardening and significant overstrength of short-length core provides significant post-yield stiffness for the braced frame and moderates residual drifts under severe earthquakes (Hoveidae et al. 2015).

Former short-length BRB conceptions suggested by Hoveidae et al. (2015) and Pandikkadavath and Sahoo (2016) included reduced-length steel plate as the core member surrounded by rectangular hollow sections. Considering construction costs, simplicity, speed of construction, and erection, it has been found that tube-in-tube BRBs offer several advantages over conventional BRBs that are normally composed of steel core plates enclosed by concrete-filled rectangular tubes (Ghasemi 2006).

Despite BRBs exhibit stable and plump hysteretic response under cyclic loading; they are susceptible to seismic loss caused by residual deformations, even after code practiced level of earthquakes (Sabelli et al. 2003). Field exploration conducted after major earthquakes (McCormick et al. 2008) revealed that many structures were no longer worth of repairing or strengthening due to excessive permanent deformation and were eventually devastated; despite they were able to survive elastic deformations during seismic events. Excessive residual deformation might also obstruct the post-event recovery of building function and warrant costly repairing work. As a result, community becomes increasingly aware of the pressing need of reducing residual deformations for structures (Christopoulos et al. 2003).

The idea of hybrid BRB was first proposed by Atlayan and Charney (2014), in which the proposed BRB decreased the residual drifts in BRBFs. However, the proposed schematic hybrid BRB conception was not supported by feasible and practical details.

The purpose of current study is to come up with an innovative scheme for all-steel BRBs to reduce residual drift and peak inter-story drift concentrations. The novelty over former proposals for residual drift mitigation is to manipulate the strain hardening features via short-length multi-material cores.

The concept of hybrid BRB including short-length cores has not yet been studied in detail. Thus, the present study is particularly interested in using short-length hybrid BRBs, owing to their proficiency to decrease residual drift demands in buckling restrained braced frames. The proposed short-length hybrid BRB (SLHBRB) comprises a hybrid core with different material arrangements and thus various strain-hardening capacities. The SLHBRB is expected to feature superior strain hardening characteristics over formerly offered hybrid or short-length BRBs. Additionally, employing a short-length core facilitates the BRB fabrication and improves the repair/replace decision after severe ground motions. The proposed SLHBRB is expected to combine individual benefits of short-length and hybrid BRBs, thus providing superior re-centering capability compared with conventional BRBs.

This paper first briefly represents the components, critical load evaluation, and design procedure for proposed SLHBRB. A finite element verification of proposed device is conducted in ABAQUS (2020). Subsequently, pushover analysis is performed on prototype multi-story BRBFs. Finally, re-centering capability of SLHBRB over conventional BRBs is evaluated through nonlinear time history analyses using OpenSEES (2007).

2 Concept of proposed SLHBRB

The rudimentary idea of hybrid brace was proposed by Saeki (1997). Recently, other scholars have numerically studied the ability of hybrid BRBs to diminish residual drifts in BRBFs (Atlayan, 2013; Jia et al. 2018; Hoveidae 2019).

The proposed SLHBRB, which is composed of a short-length hybrid BRB serially connected to a robust non-yielding (or elastic) member, is expected to compensate low post-yield stiffness of conventional simply supported BRBFs. The concept of BRB hybridity raises from using different core materials that yield at different lateral drifts. The high strain-hardening capacity of hybrid core produces significant post-yield stiffness for the BRB, thus resulting smaller residual drifts. Figure 1 represents the proposed SLHBRB components in detail. Circular hollow sections (CHSs) are assigned for the core elements and surrounding sleeve, as shown in Fig. 1. A collar is used to prevent core local buckling at the end projection. Multi-material cores, sleeve, non-yielding part, and collars are entirely made by steel circular hollow sections. Mid-plates are provided to link the cores and non-yielding part via a bolted connection. The core elements and the non-yielding part are connected to the mid-plates by groove and fillet welds, respectively. The restraining system consists of restrainer plates and circumferential disks inserted into the sleeve. Instead of concrete or mortar infill, steel restrainer plates and disks are employed to minimize the core local buckling amplitudes and transverse normal contact forces to the outer sleeve. A small gap is provided for simple placement of the restraining system inside the sleeve. Furthermore, a small clearance between the core and encasing system ensures free axial deformation and lateral expansion of the core. Likewise, independent axial deformation of individual core elements is guaranteed by a small gap provided at the interface. The restrainer plates are welded to the circumferential disks as well as the mid plate. As displayed in Fig. 1, similar section properties are assumed for the sleeve and non-yielding part. The bolted connection of circular mid-plates allows for simply replacing the damaged short-length core. The end connection of SLHBRB consists of two steel plates welded to the end plates. The gusset plate is mounted between the stiffened plates via a bolted connection, as emerges in Fig. 1e. According to tabulated values in Table 1, the hybrid core is supposed to be made by three different steel materials, including Grade 50 steel (G50) with the yielding stress of 353 MPa, Low yield point steel (LYP100) with the yielding stress of 76.5 MPa, and stainless steel 304L (SS) with the yielding stress of 252 MPa. Both LYP100 and stainless steel materials possess high strain-hardening capacities. Stainless steel is more durable and has excellent corrosion resistance. Unlike LYP100 steel, stainless steel is available in a wide variety of sizes and sections. Nevertheless, LYP100 is more ductile and has lower yielding strength, in comparison to stainless steel.

Dusicka et al. (2007) conducted experiments on G50 and LYP100 steel coupons subjected to reversed cyclic strains using a self-reacting load frame. The reduced section diameter of the coupon was maintained at 20 mm with a reduced length of 25 mm, resulting in a reduced section length to diameter ratio of 1.25. Furthermore, Beaumont and Annan (2016) experimentally evaluated the cyclic response of stainless steel 304L coupon with reduced section diameter of 16 mm and a reduced length of 28 mm. Figure 2 compares the monotonic and cyclic stress–strain responses of G50 and LYP100 provided by aforementioned researchers. As illustrated in Fig. 2, LYP100 and particularly stainless steel exhibit higher monotonic post-yield stiffness, compared with G50. Likewise, significant cyclic hardening of LYP100 and especially stainless steel compared with G50 steel is evident in Fig. 2.

As shown in Fig. 2, in contrast to G50 steel, cyclic stress–strain curves of LYP100 and stainless steel do not stabilize, which contributes to significant cyclic strain hardening. Compared with G50 steel, LYP100 steel exhibits much lower yielding capacity, higher ductility, and significantly higher ultimate strain (57%). The ultimate strain of G50 steel is around 18% in tensile test. While G50, LYP100, and stainless steels are used in this research, other material combinations for the hybrid core may also be conceivable.

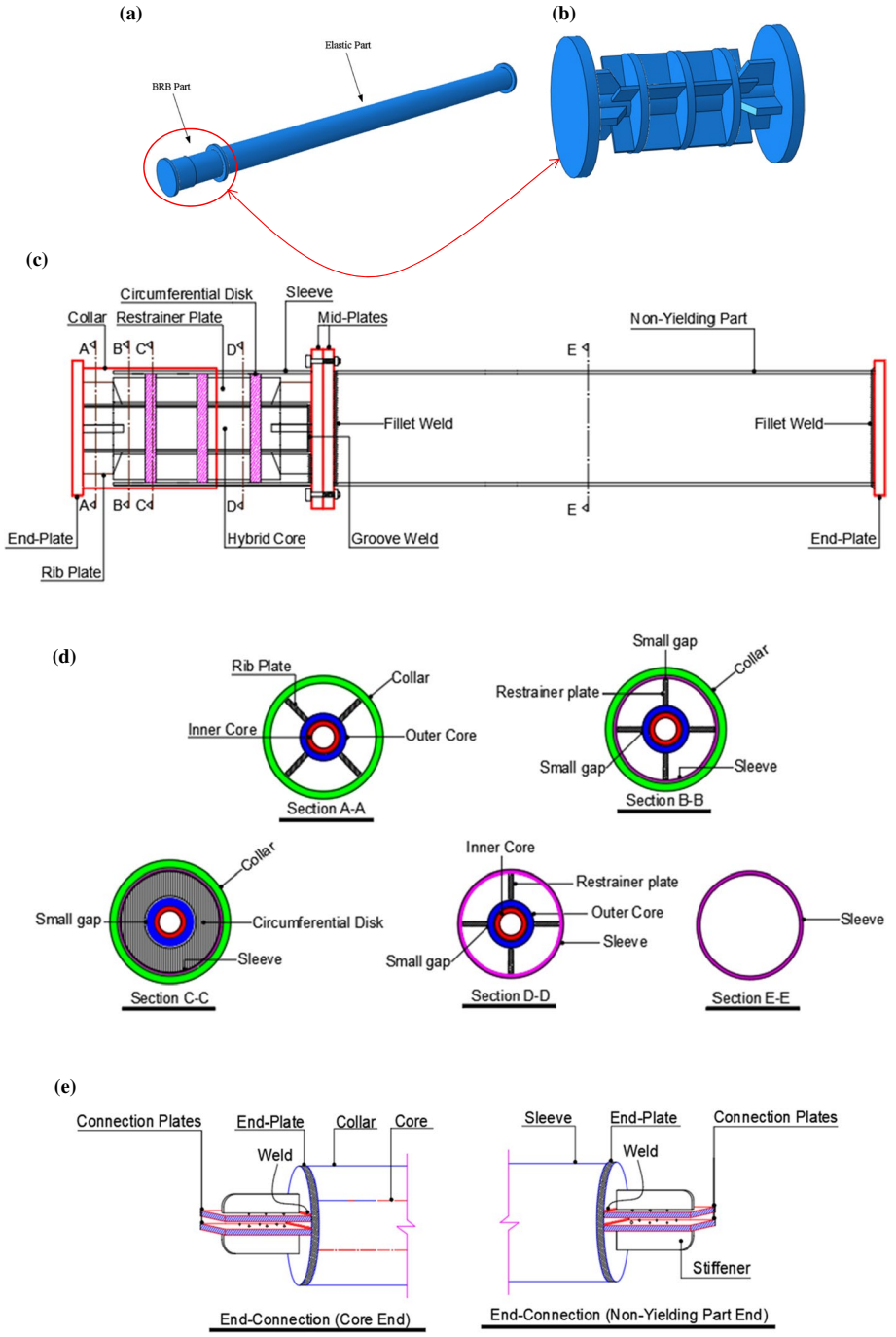

Fig.1 Proposed SLHBRB. **a** 3D view of brace, **b** a close-up of core and encasing system, **c** longitudinal view, **d** cross-sectional detail, **e** end-connection detail

Table 1 Mechanical properties of SLHBRB core materials

Material	E(GPa)	F_y(MPa)
G50	186.2	353
LYP100	153.0	76.5
SS	194.5	252

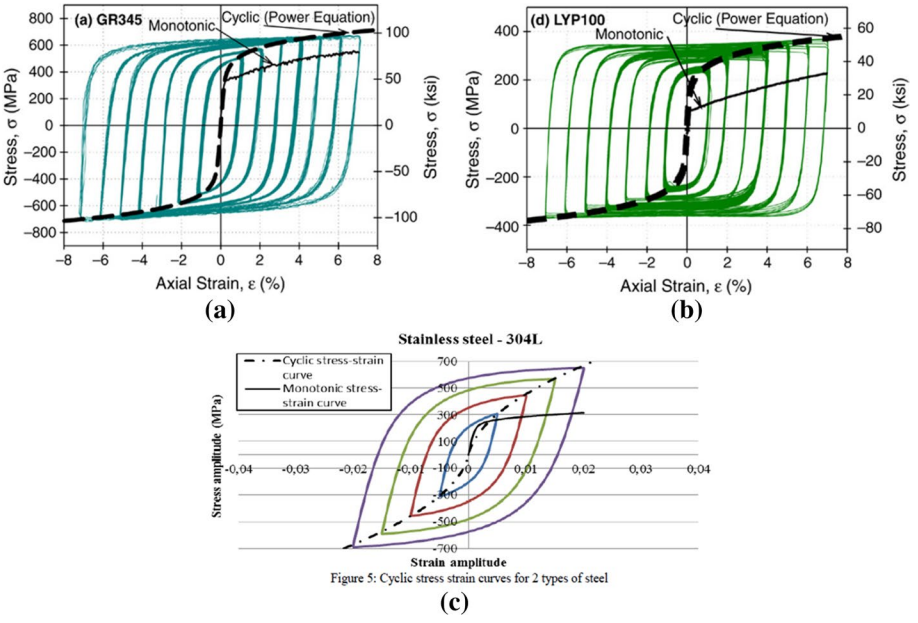

Fig.2 Stress–strain relationships of **a** G50 (GR345) steel (Dusicka et al. 2007). **b** LYP100 (Dusicka et al. 2007). **c** Stainless steel 304L (Beaumont and Annan 2016)

3 Evaluation of critical core length

As aforementioned, the proposed SLHBRB comprises decoupled reduced-length cores serially connected to a robust member. The reduced-length hybrid core is anticipated to experience large plastic deformations and high strain demands. One challenging issue in design of SLHBRB is to characterize the critical yielding length of the core. The short-length core is susceptible to low-cycle fatigue fracture (LCFF) due to high strain demands. In this paper, the well-known Coffin (1954) and Manson (1954) fracture rule was employed to estimate critical core length. AISC (2016) seismic provisions for steel structures require BRBs to be verified by a cyclic loading protocol as below:

$$\begin{aligned} &2\,\text{cycles}\ @\ \Delta = \pm\Delta_{by} \\ &2\,\text{cycles}\ @\ \Delta = \pm 0.5\Delta_{bm} \\ &2\,\text{cycles}\ @\ \Delta = \pm\Delta_{bm} \\ &2\,\text{cycles}\ @\ \Delta = \pm 1.5\Delta_{bm} \\ &2\,\text{cycles}\ @\ \Delta = \pm 2\Delta_{bm} \end{aligned} \tag{1}$$

in which Δ_{by} specifies the yielding displacement and Δ_{bm} accounts for the brace axial deformation matching design story drift (Δ_m). The design story drift can be written as below:

$$\Delta_m = C_d \cdot \Delta_E \tag{2}$$

where C_d represents the drift amplification factor, which is set to 5 for buckling restrained braced frames, according to Table 12.2-1 of ASCE (2016) regulations. In addition, Δ_E denotes the brace axial deformation corresponding to elastic story drift under design-based earthquake (DBE). Conservatively, the brace yielding displacement Δ_{by} can be specified as the upper limit for Δ_E, without conducting a linear analysis of buckling restrained braced frame. By considering above assumptions, the critical core length can be evaluated based on low-cycle fatigue fracture life of the hybrid core, under AISC loading protocol. According to Coffin and Manson findings in low-cycle fatigue regime (Uriz 2005), a linear equation in terms of the number of cycles to trigger fracture and the plastic strain amplitude can be used as follows:

$$\varepsilon_p = 2\varepsilon_f (2N_f)^c \tag{3}$$

where ε_f, and c represent material fatigue parameters and are experimentally determined. N_f and ε_p symbolize the number of cycles at the beginning of fracture and plastic strain demand in the core, respectively. Due to hybridity of core member, the critical core length was estimated separately for individual core materials. The critical material in terms of fatigue fracture life was considered as the governing material and the corresponding critical core length was designated as the critical core length of entire brace, consequently. The linear summation of damage at each cyclic deformation amplitude using Miner's rule results in the total damage index per material, as in the following:

$$\textit{Damage index} = \sum \frac{n_i}{N_{fi}} \leq 1 \tag{4}$$

where n_i and N_{fi} represent the number of cycles at each constant deformation amplitude and the total number of constant amplitude cycles required to initiate the failure, respectively. A damage index of 1.0 corresponds with the threshold of fracture. Table 2 summarizes the fatigue constants for various core materials, including G50, LYP100, and stainless steel (SS).

Table 2 Fatigue constants for core materials

Material	ε_f	c	References
G50	0.535	−0.59	Dusicka et al. (2007)
LYP100	0.275	−0.459	Dusicka et al. (2007)
SS	0.133	−0.374	Beaumont and Annan (2016)

According to Fig. 3, the proposed SLHBRB can be supposed as serially connected springs. Due to deformation compatibility, equal axial strains are expected for individual core elements in a hybrid BRB. The brace axial displacement in the elastic range can be written as the summation of axial displacement demands in hybrid core, connection parts, and non-yielding part, as follows:

$$\begin{aligned} \Delta_b &= \Delta_c + \Delta_{con} + \Delta_{el} \\ \Delta_b &= \Delta_c \left[1 + \frac{\sum_{i=1}^{n} E_{ci} A_{ci}}{E_{con} A_{con}} \cdot \frac{L_{con}}{L_c} + \frac{\sum_{i=1}^{n} E_{ci} A_{ci}}{E_{el} A_{el}} \cdot \frac{L_{el}}{L_c} \right] \end{aligned} \tag{5}$$

In Eq. (5), Δ_b and Δ_c designate the axial displacement demands of entire brace and the core member, respectively. L_c,L_{el}, and L_{con} correspondingly represent the core length, non-yielding part length, and the end-connection length. Furthermore, A_{ci}, A_{el}, A_{con}, E_{ci}, and n symbolize the cross sectional areas of the individual core members, the cross sectional area of the non-yielding part, the cross sectional area of the end connections, Young's modulus of individual core members, and number of core members in the hybrid BRB, respectively. By imposing the axial deformation, at the first phase, the core element with lowest yielding strain starts to yield. As the axial strain demand increases, yielding of the other core element with higher yielding strain triggers. The yielding of entire brace occurs at the onset of yielding in the core element with highest yielding strain capacity. It is assumed that the plasticity flows only in the core elements, while the connection and non-yielding part of the brace remain in the elastic range. Thus, the brace yielding displacement can be written in the form below:

$$\Delta_{by} = \varepsilon_{yn} \left[L_c + \frac{\sum_{i=1}^{n-1} E_{ci}^{p} A_{ci} + E_{cn} A_{cn}}{E_{con} A_{con}} L_{con} + \frac{\sum_{i=1}^{n-1} E_{ci}^{p} A_{ci} + E_{cn} A_{cn}}{E_{el} A_{el}} L_{el} \right] \tag{6}$$

in which Δ_{by}, E_{ci}^{p}, characterize the brace yielding displacement and tangent modulus of individual core materials. In addition,ε_{yn}, A_{cn}, and E_{cn} correspondingly represent yielding strain capacity, Young's modulus, and the cross sectional area of the core element with highest yielding strain. Assuming a bilinear stress–strain behavior for the core materials and considering the monotonic tests conducted by Dusicka et al. (2007), the tangent modulus ratio for G50, LYP100, and SS can be taken as 0.005, 0.016, and 0.015, respectively.

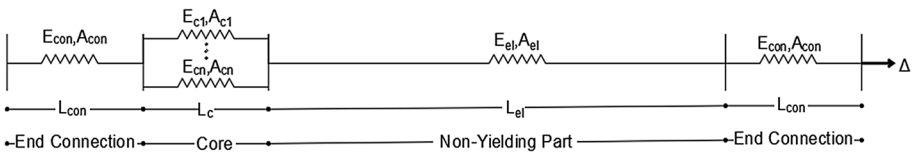

Fig. 3 Scheme of a SLHBRB as serially connected springs

While the yielding displacement is defined for the entire brace, the plastic strain demand in the core can be written in the form below:

$$\varepsilon_p = \frac{\Delta_i - \Delta_{by}}{L_c} \tag{7}$$

where ε_p, Δ_i, and L_c correspondingly represent plastic strain demand in the core, imposed axial displacement, and core length.

The following division of this paper deals with analytical evaluation of local and global responses of SLHBRBs. In order to numerically calculate Δ_{by} and critical core length L_c, and subsequently capture local and global responses of SLHBRBs, geometric characteristics of the brace member and the braced frame should be available. For this purpose, a prototype 4-story building with 3.2 m story height and four spans of 5 m in each direction was designed per Iranian codes. The building characteristics coincided with specifications of archetype building models assumed for subsequent global analyses of proposed BRBs. Afterwards, BRB components were designed and the critical core lengths were evaluated. It is noteworthy to mention that independent low-cycle fatigue fracture lives were assumed for individual core materials. By accumulating the damage over AISC (2016) standard loading protocol, critical core lengths were specified by setting the damage index to unity.

Table 3 represents the critical core lengths for different combinations of core materials. The end-connection length of SLHBRBs was obtained as 400 mm, according to preliminary design. In addition, the cross sectional area of non-yielding part was supposed to be four times that of the core. Moreover, the ratio of cross sectional area of end-connection and the core was set to 2.5 to ensure elastic response.

According to data provided in Table 3, the critical core length of short-length hybrid BRB made by G50 and LYP100 cores was specified as 665 mm. The corresponding value for the SLHBRB including stainless steel and LYP100 cores was determined as 1224 mm. The first row in Table 3 indicates the critical core length of 500 mm for the short-length BRB made by single core G50 steel material. Furthermore, the last column in Table 3 illustrates the anticipated core strain of short-length BRBs at the end of AISC (2016) standard loading protocol. As shown in Table 3, despite the short-length cores experience high strain demands, the maximum core strain remains below the fracture strain for individual materials at the end of standard loading protocol.

Table 3 Critical core length values

Core hybridity type	LCFF governing material	L_c (mm)	Δ_{by} (mm)	ε_c (%)
Non-hybrid single Core (G50)	G50	*500*	3.24	10
SLHBRB (LYP100+G50)	LYP100	*665*	3.73	8
SLHBRB (LYP100+G50)	G50	429	3.39	12
SLHBRB (SS+LYP100)	SS	*1224*	3.27	4
SLHBRB (SS+LYP100)	LYP100	676	2.71	8

4 Stability analysis and design procedure

The key parameter in design of SLHBRB is the critical core length, which can be approximated by taking into account the low-cycle fatigue fracture life of the core member under prescribed loading protocol. On the other hand, the estimation of global buckling load of the entire brace is essential for design of the SLHBRB. The hybrid core in a SLHBRB can be categorized as a displacement-controlled member. The non-yielding (i.e. elastic) part serially connected to the hybrid core is presumed to remain elastic during cyclic loading of the brace. Therefore, larger cross sectional area should be specified for it. In this paper, the ratio of cross sectional area of the elastic part and the core is set to four. The elastic part can be assumed as a force-controlled member, which is expected to sustain adjusted axial force developed in the hybrid core. Hence, it should be designed for an axial force as follows:

$$P_{\max} = \beta \cdot \omega \cdot \left(\sum_{i=1}^{n} f_{yc}^{i} \cdot A_{c}^{i} \right) \tag{8}$$

where $P_{\max}$, β, and ω represent maximum axial force developed in the elastic part, compression strength and strain hardening adjustment factors, respectively. The compression strength adjustment factor characterizes the ratio of compression and tensile strengths. In addition, the strain hardening adjustment factor determines the ratio of maximum tensile capacity and the yielding capacity of a BRB. In Eq. (8), A_c^i denotes the cross sectional area of individual core members. Furthermore, f_{yc}^i and n symbolize the yielding stress and number of core elements, respectively. The elastic part of SLHBRB is subjected to a large axial force developed in the hybrid core, and therefore is prone to buckling. Consequently, it should be designed like a buckling-type compression member. The stability analysis of SLHBRB is compulsory to predict inelastic buckling load of the elastic part. Neglecting the friction forces between sleeve and core, the total axial force developed in the hybrid core would be transmitted into the elastic part. Figure 4. signifies the overall configuration of SLHBRB along with its mathematical model. The closed-form critical load in a SLHBRB is proposed and presented in the following:

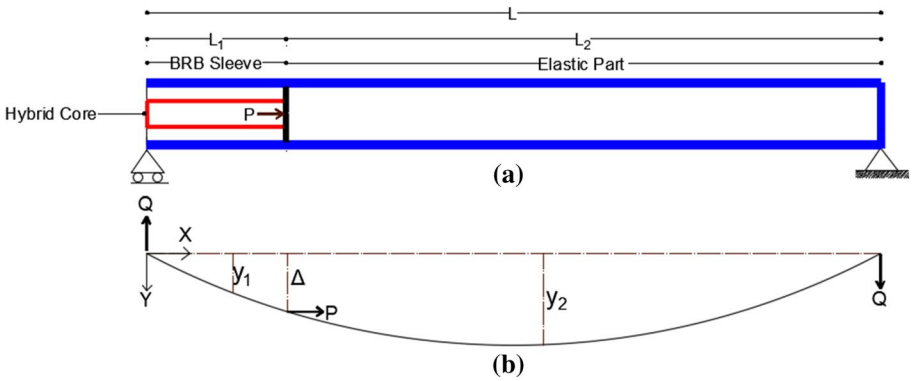

Fig. 4 **a** Schematic configuration of SLHBRB. **b** Mathematical model of SLHBRB

$$
\begin{aligned}
&Q = \frac{P\Delta}{L}\\
&-EI_1 y_1''(x) - \frac{P\Delta}{L}x = 0\\
&-EI_1 y_2''(x) - Py_2 + P\Delta\left(1 - \frac{x}{L}\right) = 0\\
&(I) \rightarrow y_1 = -\frac{P\Delta}{6EI_1 L}x^3 + C_1 x + C_2\\
&(II) \rightarrow y_2 = A\ \sin\ k_2 x + B\ \cos\ K_2 x + \frac{\Delta}{L}(L - x)\\
&\left\{\begin{array}{l} y_1(x=0) = 0 \\ y_1(x=L_1) = \Delta \end{array}\right\}\\
&\rightarrow C_2 = 0, C_1 = \frac{\Delta}{L_1}\left[1 + \frac{PL_1^3}{6EI_1 L}\right]\\
&\left\{\begin{array}{l} y_2(x=L_1) = \Delta \\ y_2(x=L) = 0 \end{array}\right\}\\
&A = \frac{\Delta\left(\frac{L_1}{L}\right)}{\sin\ k_2 L_1 - (\tan\ k_2 L)(\cos\ k_2 L_1)}, B = -A\tan k_2 L\\
&Since: y_1'\left(x = L_1\right) = y_2'\left(x = L_1\right) \rightarrow \frac{k_2 L_1}{\tan\left(k_2 L_2\right)} = \frac{PL_1^2}{2EI_1} - \frac{L}{L_1}\left[1 + \frac{PL_1^3}{6EI_1 L}\right] - 1\\
&k_2 = \sqrt{\frac{P}{EI_2}}, k_1 = \sqrt{\frac{P}{EI_2}} \rightarrow \left[\frac{K_2 L_1}{\tan\ k_2 L_2} = \frac{k_1^2 L_1^2}{3} - \frac{L}{L_1} - 1\right]
\end{aligned}
\tag{9}
$$

in which, P, Δ, I_1, and I_2 correspondingly symbolize the brace axial load, deflection of the mid-connection, moment of inertia of the restraining system, and moment of inertia of the non-yielding segment. Equation (9) can be solved numerically to calculate the critical load of the SLHBRB. While the elastic buckling load is determined, the non-yielding part can be designed as a column considering its inelastic buckling capacity, according to the design procedure proposed for short-length BRBs (Hoveidae et al. 2015).

5 Finite element verification of proposed device

To provide an analytical understanding of cyclic response of proposed BRB, finite element analysis was conducted. The BRB located at the first story of 4-story prototype frame was considered for the analysis. The procedure demonstrated in previous section was implemented to design the BRB components. Finite element model of a SLHBRB comprising G50 and LYP100 cores was built in ABAQUS finite element package. Table 4 represents the geometric characteristics of BRB model. The characteristics of FEM model coincides with proposed scheme of SLHBRB, represented in Fig. 1.

The 3D finite element model included the core, non-yielding part, end collars, ribs, disk connectors, disks, end plates, and the outer sleeve, as appears in Fig. 5.

The cores and buckling restraining components were modeled using eight node C3D8R linear brick elements with reduced integration. For accuracy of results, a mesh sensitivity

Table 4 Geometric characteristics of FEM model

Model	G50 core	LYP core	Sleeve	Elastic part	Disk	Disk connectors	End and mid-plates	Collar
SLHBRB G50+LYP100	CHS* (L*D*t) 660*61*9.1	CHS (L*D*t) 660*42*4.5	CHS (L*D*t) 600*261*6	CHS (L*D*t) 3900*261*6	D = 249 t = 20	PL t = 20	D = 350 t = 30	CHS (L*D*t) 200*285*10

*Dimensions in (mm)

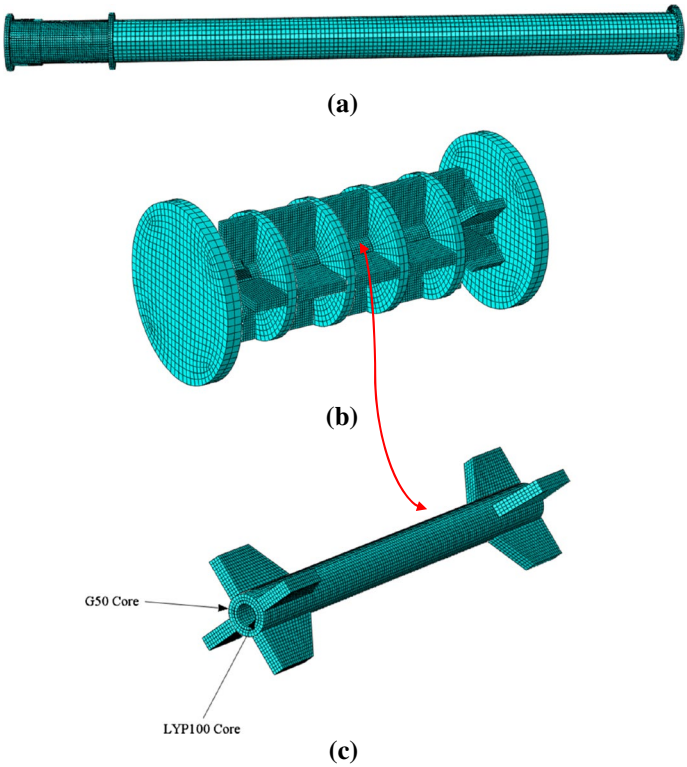

Fig. 5 FEM model of **a** Entire brace. **b** BRB part. **c** Hybrid core

analysis was performed to define the appropriate mesh density. As a result, a coarse mesh (15 mm) was employed for the elastic part, while a finer mesh (5 mm) was adopted for the BRB part. A tie interaction type was used to simulate welded connections. Large displacement static cyclic analysis was performed and the full Newton–Raphson method was considered for solving nonlinear equations. In addition, maximum and minimum increment sizes of 0.5 and 1E-6, respectively, were specified in the analysis. Contact properties with tangential Coulomb frictional behavior were assumed between multi-material cores and the buckling restraining components. To this aim, a smooth contact interaction was employed between G50 and LYP100 cores. Similar contact properties were assumed between the outer core element and the restraining system. Despite the debonding agent was not explicitly modeled, a friction coefficient of 0.04 was adopted to simulate steel-PTFE contact surfaces. Furthermore, a friction coefficient of 0.5 was adopted for steel-steel contacts. A hard contact rule was assumed for the normal direction, which minimized the penetration of the core and encasing surfaces. The contact model allowed for the separation of core from encasing member, which enabled higher mode buckling of the core. A nonlinear combined isotropic-kinematic hardening rule characterized in Table 5, was employed to reproduce the inelastic material property and therefore an accurate cyclic response. It should be noted that G50 and LYP100 steel materials were adopted for core elements. Likewise, for other components including sleeve, elastic part, disks, disk connectors, end plates, and ribs, a G50 steel material was assumed.

Table 5 Components of combined hardening material model

Material	G50	LYP100
E (MPa)	186,200	153,100
σ_0 (MPa)	353	76.5
C_1^* (MPa)	41,513	8000
γ_1	697	400
C_2 (MPa)	15,152	1200
γ_2	137.5	130
C_3 (MPa)	600	2730
γ_3	4.6	100
C_4 (MPa)	255	–
γ_4	2.2	–
C_5 (MPa)	195	–
γ_5	0	–
Q_∞	110	100
b	4	8
References	Zub et al. (2019)	

An initial geometric imperfection of L/1000 using perturbation of the geometry based on the first-mode buckling pattern was considered. The axial deformation was blocked at one end of brace with a pinned connection. Axial displacements were imposed at the other end, following a cyclic quasi-static loading protocol comparable to AISC (2016) standard loading protocol. In order to reduce analysis time and cost, the loading protocol included one cycle at $\pm\Delta_y$, one cycle at $\pm 0.5\Delta_{bm}$, one cycle at $\pm\Delta_{bm}$, one cycle at $\pm 1.5\Delta_{bm}$, and one cycle at $\pm 2\Delta_{bm}$, where Δ_y corresponds to yielding displacement of brace, and Δ_{bm} is the axial deformation of the brace corresponding to the design story drift. The values of Δ_y and Δ_{bm} were set to 4.31 mm and 27 mm, respectively. A static cyclic analysis was performed and hysteretic responses of proposed BRB was well predicted by the finite element model in both elastic and nonlinear ranges. Figure 6 represents the normalized hysteretic response of the brace in which the abscissa and ordinate characterize the brace normalized axial deformation and axial force, respectively. As shown in Fig. 6, regardless of small fluctuations due to local buckling of hybrid core under compression, the SLHBRB possess plumb and stable hysteretic response. Figure 7 depicts the local buckling of G50 and LYP100 cores under compression. As appears in Fig. 7, the restraining system is strength enough to

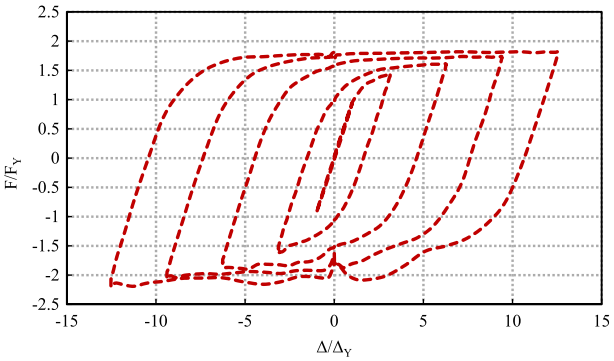

Fig. 6 Normalized hysteretic response of proposed SLHBRB

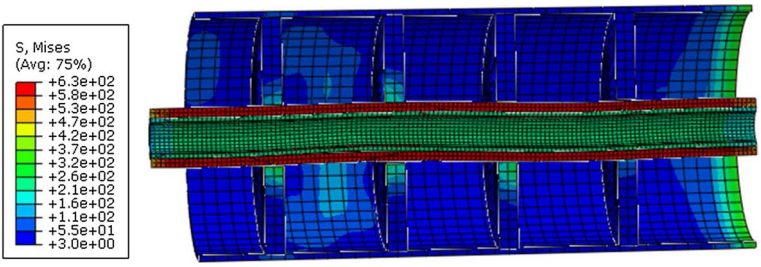

Fig. 7 Local buckling of hybrid core under compression (half-view)

hinder global buckling of the brace and diminish the core local buckling amplitudes. FEM analysis results confirmed the capability of conceptual short-length hybrid BRB to sustain large plastic deformations without any instability or significant degradation of strength and ductility.

6 Local behavior of single SLHBRB member

The main purpose of this paper is to compare the seismic demands in braced frames incorporating short-length non-hybrid BRBs, short-length hybrid BRBs (i.e. SLHBRBs), and conventional full-length BRBs. For a more accurate comparison of seismic responses, cross sectional areas of core members were adjusted so that equal yielding strengths and elastic stiffness could be achieved.

Before examining the global behavior of braced frames incorporating SLHBRBs, single BRB members were simulated in OpenSEES to acquire force–deformation relationships. Beam-column elements were assumed for brace components. The analytical model of short-length hybrid BRB included two elements connected in parallel. The hybrid core was serially connected to non-yielding member, as shown in Fig. 8. The BRB models were subjected to a monotonic displacement sequence up to 50 mm. Figure 9 illustrates and compares the force–deformation responses in full-length (G50), short-length non-hybrid (G50), and hybrid BRBs. Geometric features of BRB models are summarized in Table 6. For simplicity, the core cross sectional area of full-length BRB, A, was set to unity and the core cross sectional areas of other models were adjusted according to Table 6. As it can be understood from Fig. 9, BRB models, having equal yielding strengths, exhibit different post-yield stiffness. The elastic axial stiffness of full-length BRB is considerably smaller in comparison to short-length BRBs. Due to higher strain-hardening capacity, the post-yield

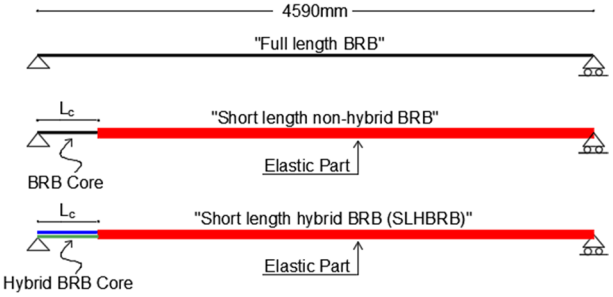

Fig. 8 OpenSEES models of single BRBs

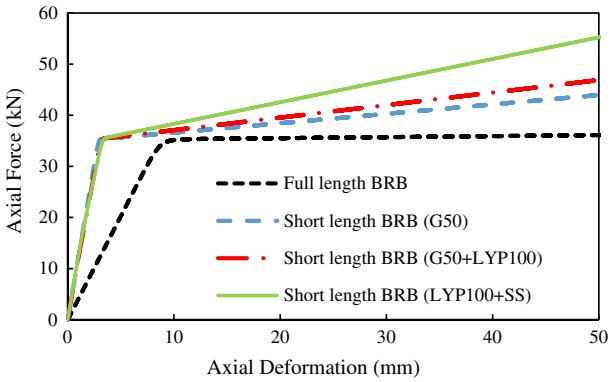

Fig. 9 Force–deformation responses of BRB elements

Table 6 Geometric specifications of single BRBs

BRB type	L_c(mm)	L_{el}	L_{con}	A_c	A_{el}	A_{con}
Full-length BRB (G50)	4590	*	400	A	*	2.5 A
Short-length BRB (G50)	500	4090	400	A	4 A	2.5 A
SLHBRB (G50 + LYP100)	660	3930	400	$A_{G50} = 0.927A$	4 A	2.5 A
				$A_{LYP100} = 0.338A$	4 A	2.5 A
SLHBRB (LYP100 + SS)	1220*	3370	400	$A_{LYP100} = 0.756A$	4 A	2.5 A
				$A_{SS} = 1.176A$	4 A	2.5 A

*Dimensions in mm

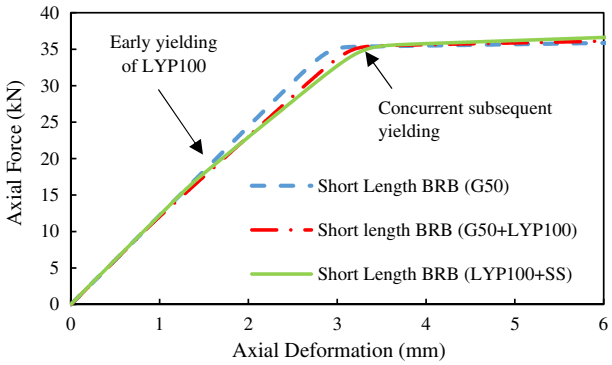

Fig. 10 Force–deformation relationships for single BRB elements at small deformations

stiffness of short-length hybrid BRBs is considerably greater in comparison to non-hybrid short-length and full-length BRBs. The hybrid BRB composed of stainless steel and LYP100 cores displays significant post-yield stiffness as shown in Fig. 9. In addition, as illustrated in Fig. 10, in small axial strains, hybrid BRBs exhibit a tri-linear force–deformation response owing to different yielding strengths of core materials. The double-stage yielding pattern involves early yielding of LYP100 steel. Subsequent yielding occurs in stainless steel and G50 steel, as shown in Fig. 10.

7 Global response of braced frames incorporating SLHBRBs

7.1 Design of prototype buildings

In order to evaluate the capability of proposed SLHBRB to mitigate seismic drifts in simply supported BRBFs, 4-story, 10-story, and 15-story prototype buckling restrained braced frames were considered. The maximum allowable structure height for simply supported buckling restrained braced frames is 50 m, according to Iranian building codes (2014). This permits having structures with designated story ranges and at most 15 stories. A rectangular-shaped plan including four bays of 5 m in each direction and typical story height of 3.2 m was supposed. The work-point to work-point length of braces was specified as 5940 mm, according to geometric specification of the braced frames. Moreover, end-connection length of 400 mm and joint length of 270 mm were assumed for SLHBRBs and conventional BRBs. Figure 11 depicts the components of BRBs in analytical models.

In order to investigate the re-centering capacity of SLHBRBs, four brace models including conventional full-length BRB, short-length single core BRB (G50), short-length hybrid BRB made by G50 and LYP100 steels, and short-length hybrid BRB including stainless steel and LYP100 cores were assumed. The geometric characteristics of BRBs inside the braced frames were analogous to those of single BRB elements represented in Table 6.

By numerically solving the stability equation for short-length BRBs, it was resulted that the assumed cross sectional area ratio for the elastic part (i.e. four) guarantees its stability and strength. The compression strength and strain hardening adjustment factors, β and ω were supposed to be 1.3 and 1.5, respectively, while designing the elastic part.

In order to compare the seismic performance of BRBFs incorporating SLHBRBs and conventional BRBs, first the prototypes were modeled and designed in Etabs software (2016). 4-story, 10-story and 15-story diagonally braced residential buildings located on type III soil in a very high seismicity zone with a PGA of 0.35 g were considered. Composite steel deck floor system with dead and live loads of 3.5 and 3.8 kN/m^2, respectively, was assumed. Moreover, dead and live loads of 3 and 1.5 kN/m^2 were specified for the roof. The external and the internal partition walls were supposed to impose dead loads of 1.5 kN/m^2 and 1 kN/m^2, respectively. The G50 steel material was assumed for all beams and columns. At the first step, the prototype buildings incorporating full-length BRBs were designed per Iranian standard codes. As a result, BRB core areas

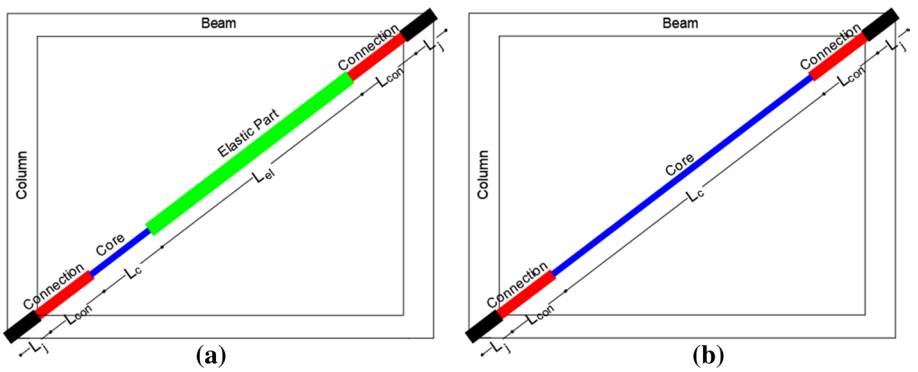

Fig. 11 Characteristics of analytical models; **a** short-length BRBs, **b** full-length BRBs

were determined considering prescribed loading combinations. Afterwards, the prototypes including single core (G50) short-length BRBs with a core length of 500 mm were modeled and designed similar to full-length BRBs. The length of elastic part in short-length single core BRB was set to 4090 mm as per Table 6. It was expected that the axial stiffness of BRBs and subsequently the lateral stiffness of the braced frames were increased while reducing the core length. According to Iranian seismic code, whenever the analytical period of structure exceeds 1.25 times of empirical period value, the empirical period can be supposed as fundamental period to evaluate base shear. According to Table 7, empirical code-based periods of the BRBFs including full-length and short-length BRBs controlled the design. Hence, equal seismic demands were assumed for the buildings equipped with full-length and short-length single-core BRBs, which resulted similar beams, columns, and BRB core areas. Figure 12 illustrates the plan view and elevation of prototype buildings. In addition, Table 7 summarizes the seismic data of prototype models. Moreover, Table 8 represents member sizes in buckling restrained braced frames. Tabulated R and C values in Table 7 symbolize the response modification factor and base shear coefficient, respectively. Considering equal lateral strength and stiffness for all BRBFs, there was no need to design the BRBFs incorporating SLHBRBs and therefore, similar beams, columns, and BRB core areas were specified for BRBFs including SLHBRBs and full-length BRBs.

7.2 Description of OpenSEES models

Two-dimensional analytical models of 4-story, 10-story, and 15-story BRBFs were built in OpenSEES software. As shown in Fig. 12a, the middle frame C was selected for the analysis. The geometric specifications of structural elements were specified according to Tables 6 and 8. Nonlinear-beam-column elements were identified for beams, columns, and braces. The analytical model of braces included all components serially connected together, as illustrated in Fig. 11. A pinned connection utilizing Zerolength element was specified at beams, columns, and brace ends. Dummy columns as elastic-beam-column elements, having moments of inertia and cross sectional areas considerably larger than frame columns, were employed to account for P-Δ effects, as shown in Fig. 13. Zerolength rotational spring elements with small stiffness were used to connect dummy columns to beam-column joints. Rigid links using truss elements were responsible for connection of dummy columns and the main frame, thus transferring the P-Δ effects. The beam elements were supposed to sustain gravity loads tributary to the frame members, while the remaining gravity loads were applied to the leaning columns.

Inherent damping was modeled by Rayleigh damping (mass and last-committed stiffness proportional model) via setting the critical damping ratio to 2% at the fundamental and third vibration modes of the structure. Steel02 material model was specified for beams and columns. The strain hardening parameters of various core materials were introduced based on the calibration data represented in Fig. 14. In SLHBRB models, different core elements were connected in parallel. The rigid diaphragm at the story levels was modeled using the constraint of equal degree of freedom of story nodes. A lumped mass system was considered in dynamic time history analysis. Linear geometric transformation was specified for brace components to ensure axial deformation of brace components. In addition, a large moment of inertia was assumed for the brace components to inhibit global buckling. Furthermore, P-δ geometric transformation was assigned for beams and columns.

Table 7 Seismic data of BRBF models

Seismic parameters	4-story		10-story		15-story	
PGA (g)	0.35		0.35		0.35	
R	7		7		7	
C	0.14		0.12		0.09	
Period (s)	Full-length	Short-length	Full-length	Short-length	Full-length	Short-length
$T_{empirical}$ (s)	0.34	0.34	0.67	0.67	0.91	0.91
$1.25T_{empirical}$ (s)	0.42	0.42	0.83	0.83	1.13	1.13
$T_{analytical}$ (s)	0.82	0.57	1.50	1.17	2.14	1.75

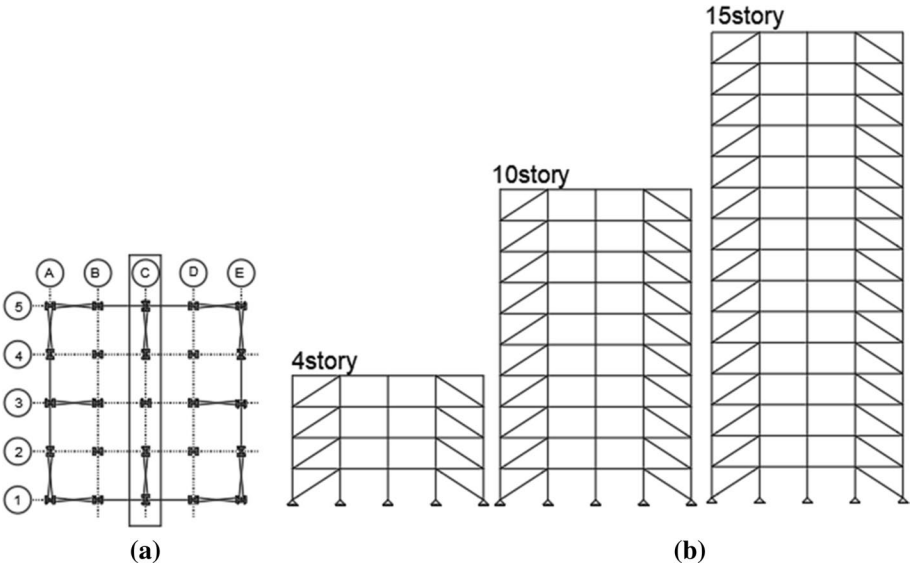

Fig.12 **a** Plan view, **b** elevation view of buckling restrained braced frames

7.3 Material calibration

Steel material calibration is essential to accurately capture and compare the response of SLHBRBs and conventional BRBs. For this purpose, past experimental data was used to calibrate steel material parameters. The analytical model of a single BRB element was built in OpenSEES and was subjected to the prescribed loading pattern. The response curves resulted from analytical and former laboratory tests were compared, subsequently. The material model parameters were changed in a way so that the test and simulation response curves approximately met together. The calibrations of G50 and LYP100 steels for monotonic loading pattern were conducted using experimental data reported by Dusicka et al. (2007). In addition, experimental data from Beaumont and Annan (2016) was utilized to calibrate stainless steel parameters. Steel02 material model was adopted for monotonic response of core materials. Figure 14 represents the calibration of G50, LYP100, and stainless steel for monotonic response using Steel02 material model. To simulate cyclic response of steel materials, Ramberg–Osgood material model was adopted for G50 and LYP100, using calibrated parameters reported by Dusicka et al. (2007). Likewise, Ramberg–Osgood model parameters suggested by Beaumont and Annan (2016) were used for stainless steel. Due to inherent difference between cyclic and monotonic strain–stress responses of steel materials, Ramberg–Osgood and Steel02 calibrated model parameters were employed to conduct nonlinear time history and static pushover analyses, respectively.

7.4 Pushover analysis

To achieve an overall understanding on the global response of BRBFs, the displacement-based monotonic pushover analyses of prototype braced frames equipped with full-length BRBs,

Table 8 Member sizes of BRBFs

Model	Story	Column	Beam	BRB core area (cm^2)
4-Story	1	W12×53	W12×19	16
	2	W12×53	W12×19	14
	3	W12×35	W12×19	12
	4	W12×35	W12×19	7
10-Story	1	W12×230	W12×19	36
	2	W12×230	W12×19	36
	3	W12×230	W12×19	36
	4	W12×136	W12×19	34
	5	W12×136	W12×19	32
	6	W12×136	W12×19	28
	7	W12×136	W12×19	24
	8	W12×50	W12×19	20
	9	W12×50	W12×19	14
	10	W12×50	W12×19	8
15-Story	1	W14×426	W12×19	44
	2	W14×426	W12×19	42
	3	W14×426	W12×19	42
	4	W14×342	W12×19	42
	5	W14×342	W12×19	42
	6	W14×342	W12×19	42
	7	W14×233	W12×19	42
	8	W14×233	W12×19	38
	9	W14×233	W12×19	38
	10	W14×159	W12×19	38
	11	W14×159	W12×19	38
	12	W14×159	W12×19	38
	13	W14×82	W12×19	38
	14	W14×82	W12×19	30
	15	W14×82	W12×19	20

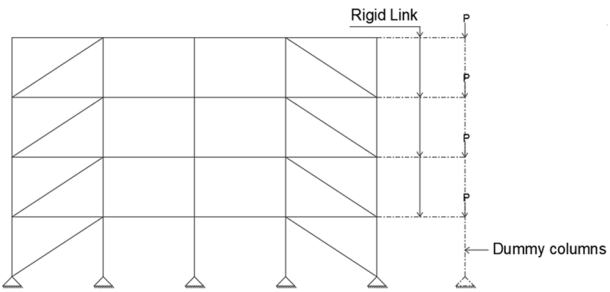

Fig. 13 The sketch of two-dimensional BRBF model in OpenSEES

short-length BRBs, and short-length hybrid BRBs were conducted in OpenSEES. A triangular loading pattern was assumed for pushover analysis. The pushover analysis was monitored by a control node at the roof level and was completed as the roof drift ratio reached to 2%.

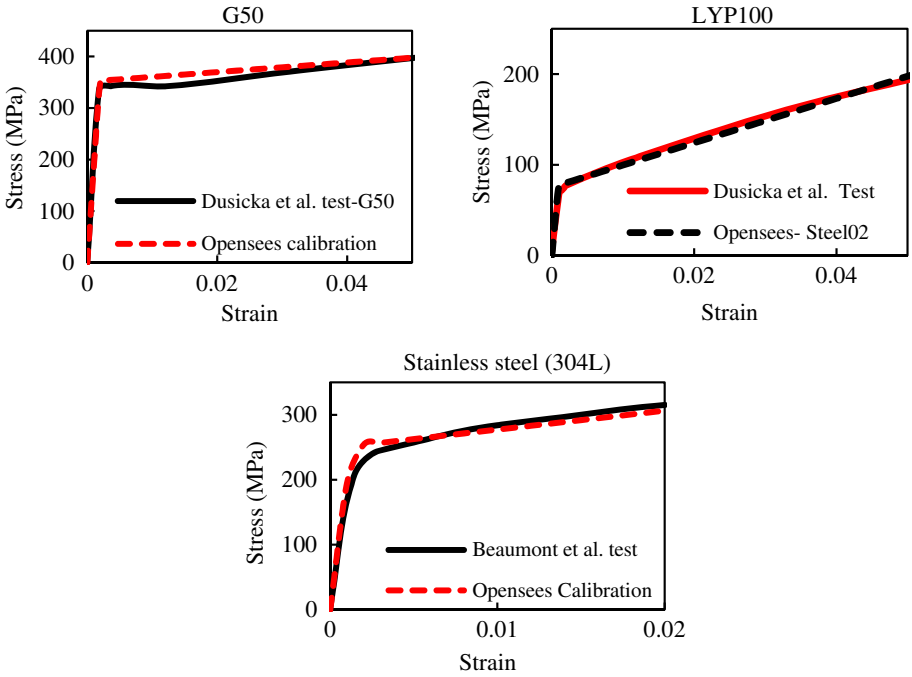

Fig.14 Calibration of core materials

Figure 15a–c represent the pushover curves, which build the relationship between the roof drift ratio and the total base shear.

As shown in Fig. 15, the lateral elastic stiffness of braced frames equipped with full-length BRB is considerably smaller in comparison to other models. In other words, reducing the core length provides significant axial stiffness for BRBs and the braced frame, as a result. Generally, due to P-Δ effects, the post-yield stiffness of structural systems tends to decrease. As shown in Fig. 15a–c, in full-length BRBFs, the post-yield slope of the pushover curve is descending. However, a positive post-yield stiffness is achieved for the braced frames equipped with short-length non-hybrid and hybrid BRBs. Thus, buckling restrained braced frames composed of short-length BRBs do not exhibit capacity degradation due to P-Δ effects. Furthermore, the core material combination affects the post-yield stiffness of the braced frame. The maximum post-yield stiffness belongs to BRBFs including hybrid core comprising stainless steel and LYP100, which can be attributed to higher strain-hardening capacity of that model. Considering Fig. 15a–c, the maximum ratio of post-yield stiffness of braced frames incorporating hybrid and non-hybrid short-length BRBs is close to 2.5.

Overall, SLHBRBs significantly enhance the post-yield stiffness and stability of simply supported buckling restrained braced frames, thus mitigating the capacity degradation due to P-Δ effects.

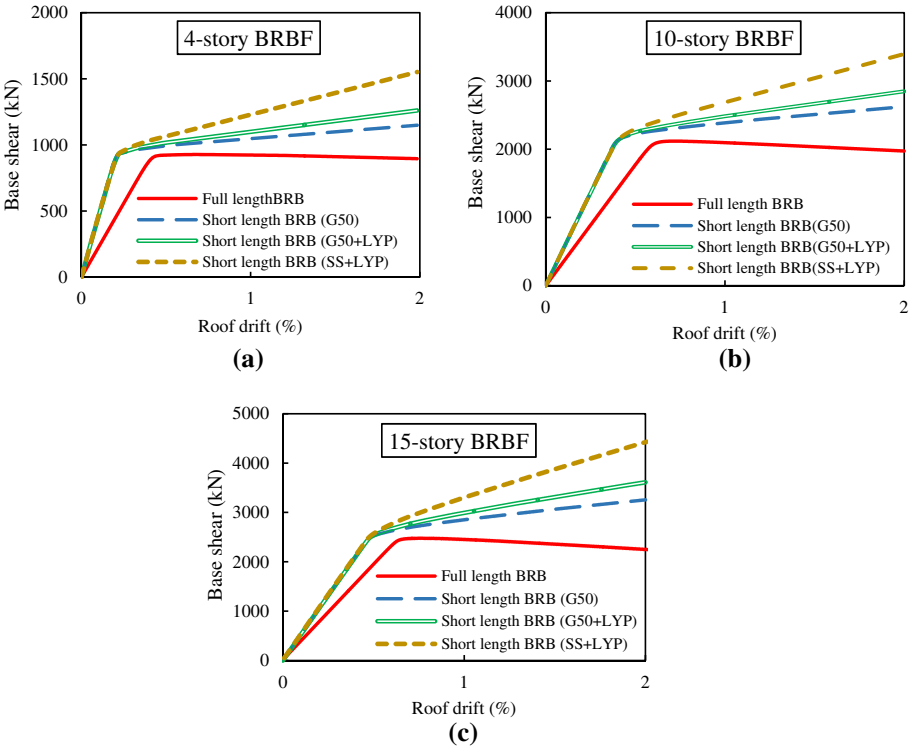

Fig. 15 Pushover curves for prototype buckling restrained braced frames

7.5 Nonlinear time history analysis

7.5.1 Record selection and matching

Nonlinear time history analysis is a powerful tool to acquire dynamic structural response under time-varying loading protocols, considering structural geometry and materials nonlinearity. For this purpose, the dynamic equilibrium equations are numerically solved by several methods like direct integration or modal techniques. The size of step time may noticeably affect the structural responses in direct-integration methods. Therefore, the step time should be reduced until results are not affected. In order to assess the seismic response of building structures, the structural models are subjected to a set of real or synthetic ground motion records. The precision of analysis results is generally influenced by record dispersion and scaling. An appropriate number of seismic records is compulsory to perform time history analysis. The Iranian seismic code regulations necessitate at least seven seismic records to conduct time history analysis. The seismic records should have seismological features analogous to the site specific expected earthquake. Therefore, it is not easy to find records that fulfill simultaneously all conditions such as magnitude, distance, fault mechanism, and soil conditions. In this paper, twenty-two far-field ground motion record set suggested by ATC-63 (2008) were employed. The record characteristics are summarized in Table 9. It should be noted that only one component of seismic records

Table 9 Specification of ground motion records

Record no	Magnitude	Year	Event name	PGA_{max} (g)	PGV_{max} (cm/s)
1	6.7	1994	Northridge	0.52	63
2	6.7	1994	Northridge	0.48	45
3	7.1	1999	Duzce, Turkey	0.82	62
4	7.1	1999	Hector Mine	0.34	42
5	6.5	1979	Imperial Valley	0.35	33
6	6.5	1979	Imperial Valley	0.38	42
7	6.9	1995	Kobe, Japan	0.51	37
8	6.9	1995	Kobe, Japan	0.24	38
9	7.5	1999	Kocaeli, Turkey	0.36	59
10	7.5	1999	Kocaeli, Turkey	0.22	40
11	7.3	1992	Landers	0.24	52
12	7.3	1992	Landers	0.42	42
13	6.9	1989	Loma Prieta	0.53	35
14	6.9	1989	Loma Prieta	0.56	45
15	7.4	1990	Manjil, Iran	0.51	54
16	6.5	1987	Superstition Hills	0.36	46
17	6.5	1987	Superstition Hills	0.45	36
18	7	1992	Cape Mendocino	0.55	44
19	7.6	1999	Chi-Chi, Taiwan	0.44	115
20	7.6	1999	Chi-Chi, Taiwan	0.51	39
21	6.6	1971	San Fernando	0.21	19
22	6.5	1976	Friuli, Italy	0.35	31

(with greatest PGA) was considered to match the design-based earthquake. According to Iranian seismic code (2007), the selected record set should be scaled in a way so that the average spectrum matches the DBE spectrum. Several approaches exist in the literature for scaling the records. Beside the present record scaling techniques, record matching is widely used. Spectral matching approach, which is used in the present study, is defined as the modification of a real seismic record in a way that its response spectrum coincides with a preferred target spectrum across a period range (0.2–1.5 T). Seismomatch (2016) is a powerful software to adjust a set of ground motion records to match a certain target spectrum. The matching procedure is conducted by wavelet algorithms without changing the frequency content of the records. Figure 16 illustrates a sample of record matching procedure conducted for 4-story BRBF.

7.5.2 Time history analysis results

The seismic response of BRBFs incorporating different BRB devices were evaluated by subjecting them to the realistic ground motion records characterized in Table 9. The structural responses including peak inter-story drift ratios (ISDRs) and residual drift ratios (RDRs) were acquired, consequently. The peak ISDR and RDR values were determined as the average of peak drifts under individual seismic records. Figure 17a–x characterize the ISDR and RDR distributions together with mean (i.e. AVE)

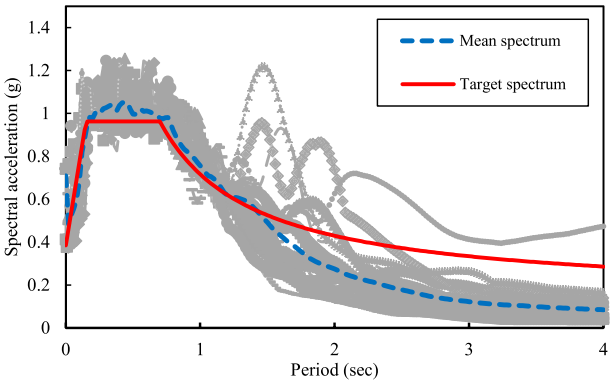

Fig. 16 A sample of spectral matching conducted for 4-story (full-length) BRBF

and AVE ± STD values, where STD denotes the standard deviation. Table 10 summarize the peak ISDR and RDR demands. Additionally, RDR and ISDR reduction percentages in BRBFs incorporating short-length non-hybrid and hybrid BRBs, respect to conventional BRBFs, are tabulated in Table 10.

According to data provided in Table 10, compared to the braced frames comprising full-length BRBs, BRBFs equipped with short-length BRBs exhibit significantly smaller ISDR and especially RDR responses. The minimum ISDR belongs to SLH-BRB model including stainless steel and LYP100 cores. In detail, in 4-story, 10-story, and 15-story BRBFs, the maximum reduction of ISDR values in BRBFs incorporating short-length BRBs, respect to conventional BRBFs, are 58%, 47%, and 44%, respectively. The corresponding RDR reduction values are 78%, 80%, and 80%, respectively. It is conspicuous that the core hybridity significantly reduces ISDR and particularly RDR demands. However, the reduction amount is directly affected by the material combination in hybrid core. Results show that hybrid BRBs made by stainless steel and LYP100 cores; having equal yielding capacity and elastic stiffness to other types of short-length BRBs, considerably decrease ISDR and RDR demands. This can be related to high post-yield stiffness of BRBFs composed of stainless steel and LYP100 steel cores, as shown in Fig. 15. In other words, the greater the post-yield stiffness, the smaller the residual drifts in BRBFs. Moreover, the results designate that RDR and ISDR demands in the braced frames comprising short-length BRBs are smaller compared with conventional full-length BRBFs. This is primarily due to high strain hardening and over-strength capacity of reduced-length cores. Likewise, the significant RDR reduction in short-length hybrid BRBFs is principally due to the significant cyclic strain hardening capacity and over-strength of stainless steel and LYP100 steel, in comparison to G50 steel.

According to analysis results, SLHBRBs may offer the engineers a new solution to diminish unacceptable residual drifts of ordinary buckling restrained braces frames. Beside the re-centering attraction of SLHBRBs, the reduced-length core element is easier to be fabricated, inspected, and replaced after large plastic deformations. Future investigations may focus on experimental evaluation of SLHBRBs, by taking into account various core materials. Moreover, upcoming investigations may encompass accurate estimation of critical core length in SLHBRBs, utilizing further low-cycle fatigue models.

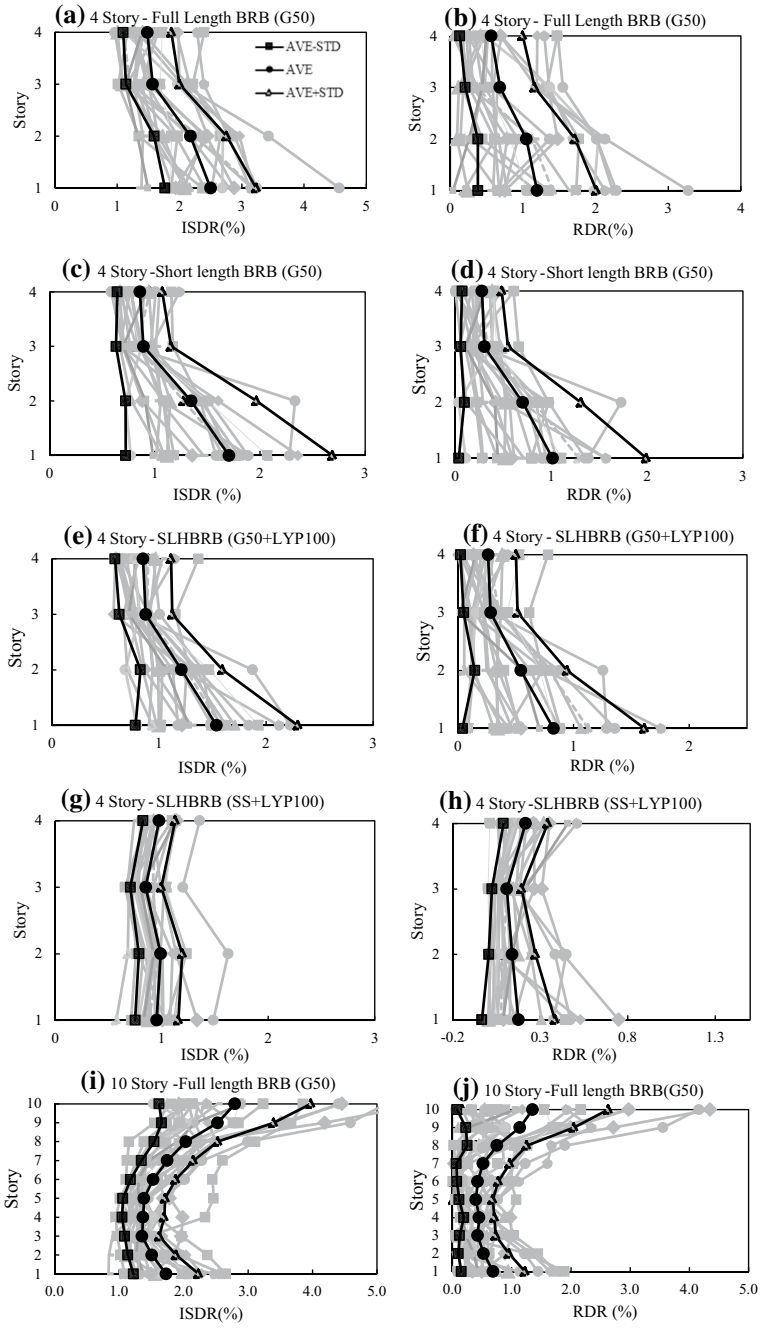

Fig. 17 Height-wise distribution of ISDR and RDR demands

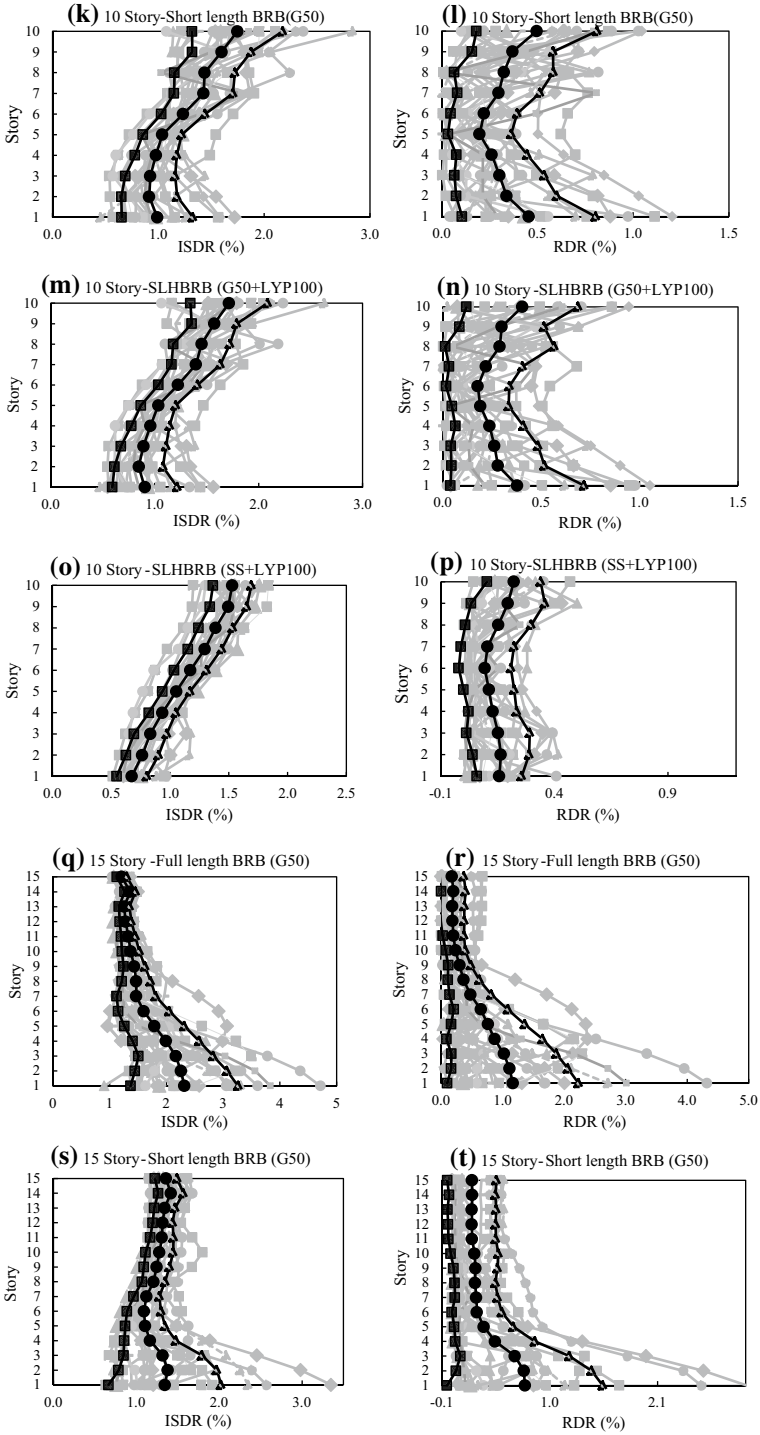

Fig. 17 (continued)

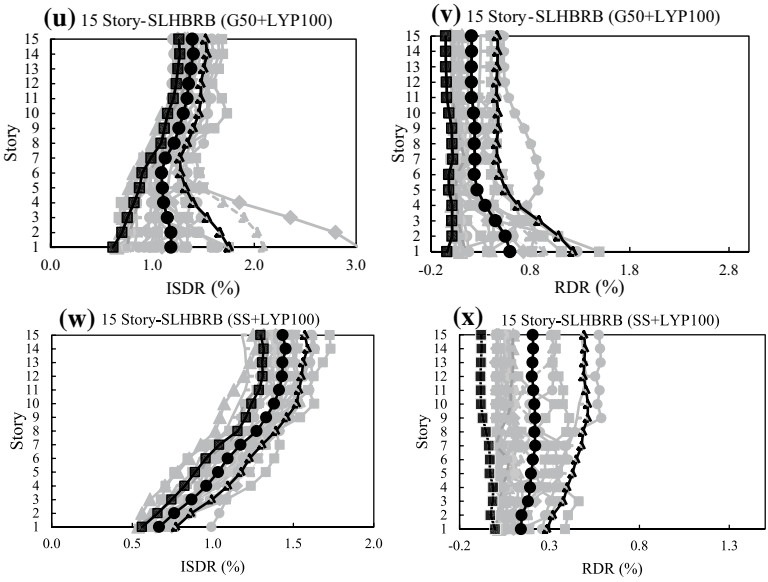

Fig. 17 (continued)

Table 10 Output of nonlinear time history analyses

BRBF model	ISDR (%)	RDR (%)	ISDR reduction (%)	RDR reduction (%)
4-Story				
Full length BRB (G50)	2.55	1.33	*	*
Short length BRB (G50)	1.72	1.06	33	20
SLHBRB (G50 + LYP100)	1.55	0.86	39	36
SLHBRB (SS + LYP100)	1.06	0.31	58	78
10-Story				
Full length BRB (G50)	2.93	1.73	*	*
Short length BRB (G50)	1.85	0.75	37	57
SLHBRB (G50 + LYP100)	1.83	0.67	38	61
SLHBRB (SS + LYP100)	1.55	0.32	47	80
15-Story				
Full length BRB (G50)	2.64	1.50	*	*
Short length BRB (G50)	1.67	0.86	37	43
SLHBRB (G50 + LYP100)	1.53	0.68	42	55
SLHBRB (SS + LYP100)	1.47	0.31	44	80

8 Summary and conclusions

The current paper introduces a novel all-steel BRB to reduce peak and residual drifts in buckling restrained braced frames. The proposed device combines individual benefits of short-length and hybrid BRBs. The study designates the advantages of proposed brace

over conventional BRBs to diminish inter-story and especially residual drifts. Nonetheless, due to significant high strain hardening and over-strength capacity of the proposed BRB, special considerations should be taken for design of force-controlled elements including end connections and columns. Finite element analysis results highlighted the capability of proposed device to sustain large plastic deformation without instability or significant degradation of capacity. Furthermore, Nonlinear time history analyses results confirmed the feasibility and revealed the intended re-centering capability of the proposed brace, offering engineers a new device to reduce residual drifts in simply supported BRBFs. Following conclusion can be drawn in the current study:

1. SLHBRBs exhibit multi-stage yielding pattern and significant post-yield stiffness. The early yielding of LYP100 contributes to high seismic energy dissipation. In addition, high strain-hardening characteristics of stainless steel and LYP100 provide significant over-strength in SLHBRB, resulting considerable re-centering capability, in comparison to conventional BRBs.
2. BRBFs equipped with properly designed SLHBRBs show significant post-yield lateral stiffness, owing to remarkable over-strength and strain-hardening capacities of hybrid core. According to pushover analysis results, the BRBFs including short-length non-hybrid and especially hybrid BRBs, display positive post-yield stiffness, without significant degradation of capacity due to P-Δ effects.
3. Nonlinear time history analyses results ascertained outstanding re-centering capability of SLHBRBs over conventional BRBs. 4-story, 10-story, and 15-story buckling restrained braced frames equipped with SLHBRBs composed of LYP100 and stainless steel cores, were found to experience 58%, 47%, and 44% smaller inter-story drifts, in comparison to conventional BRBs. However, the primary concern was the ability of SLHBRB to decrease residual drift demands and to reduce the building post-earthquake repair costs. The SLHBRBs remarkably decreased the residual drifts by 80%, which could be principally attributed to higher post-yield stiffness, compared with conventional BRBs. Finally, owing to higher initial (i.e. elastic) and post-yield stiffness compared with conventional BRBs, the proposed device can be incorporated to steel or RC frames to limit structural and non-structural damages and diminish inter-story and especially permanent drifts under moderate to severe earthquakes.

References

ABAQUS (2020) Abaqus Documentation. Dassault Systems, Waltham

AISC (American Institute of Steel Construction) (2016) Seismic provisions for structural steel buildings. Chicago, IL

American Society of Civil Engineers (ASCE) (2016) Structural engineering institute (SEI), minimum design loads for buildings and other structures. American Society of Civil Engineers/Structural Engineering Institute, Reston

ATC 63 (2008) Quantification of building seismic performance. FEMA Project, U.S.

Atlayan O (2013) Hybrid steel frames. Ph.D. dissertation, Virginia Tech.

Atlayan O, Charney F (2014) Hybrid buckling-restrained braced frames. J Constr Steel Res 96:95–105

Avci-Karatas C, Celik OC, Eruslu O (2019) Modeling of buckling restrained braces (BRBs) using full-scale experimental data. KSCE J Civ Eng 10:4431–4444

Beaumont E, Annan CD (2016) cyclic response of structural stainless steel plate under large inelastic strains. Proceeding of Resilient Infrastructure, London

Christopoulos C, Pampanin MJ, Priestley N (2003) Performance-based seismic response of frame structures including residual deformations part I: single degree of freedom systems. J Earthq Eng 7(01):97–118
Coffin LF Jr (1954) A study of the effects of cyclic thermal stresses on a ductile metal. Trans ASME 76:931–950
Della Corte G, D'Aniello M, Landolfo R (2014) Field-testing of all-steel buckling-restrained braces applied to a damaged reinforced concrete building. Journal of structural engineering 141
Dusicka P, Itani AM, Buckle IG (2007) Cyclic response of plate steels under large inelastic strains. J Constr Steel Res 63:156–164
Etabs (2016) the ultimate integrated software package for the structural analysis and design of buildings. CSI Corporations, U.S.
Fahnestock LA, Sause R, Ricles JM (2003) Analytical and experimental studies on buckling restrained braced composite frames. Proc Int Work Steel Concr Compos Constr 177–188
Fahnestock LA, Ricles JM, Sause R (2007) Experimental evaluation of a large-scale buckling-restrained braced frame. J Struct Eng 133:0733–9445
Ghasemi S (2006) The introduction of a buckling restrained bracing system for steel structures. Thesis, Under Supervision of Shahrokh Maalek School of Civil Engineering, College of Engineering, University of Tehran, Iran
Ghowsi AF, Sahoo DR (2018) Seismic performance assessment of hybrid self-centering buckling restrained braced frame systems. In: Ninth international conference on advances in steel structures (ICASS'2018), Hong Kong, China
Hosseinzadeh SH, Mohebi B (2016) Seismic evaluation of all-steel buckling restrained braces using finite element analysis. J Constr Steel Res 119:76–84
Hoveidae N (2019) Numerical investigation of seismic response of hybrid buckling restrained braced frames. Period Polytech Civ Eng 63:130–140
Hoveidae N, Rafezy B (2012) Overall buckling behavior of all-steel buckling restrained braces. J Constr Steel Res 79:151–158
Hoveidae N, Tremblay R, Rafezy B, Davaran A (2015) Numerical investigation of seismic behavior of short-core all-steel buckling restrained braces. J Constr Steel Res 114:89–99
Iranian Code of Practice for Seismic Resistant Design of Buildings (2014) Standard No. 2800, 4th Edition building and housing research center, Tehran, Iran
Jia LJ, Li RW, Xiang P, Zhou DY, Dong Y (2018) Resilient steel frames installed with self-centering dual-steel buckling-restrained brace. J Constr Steel Res 149:95–104
Kersting RA, Fahnestock LA, López WA (2015) Seismic design of steel buckling restrained braced frames—a guide for practicing engineers NEHRP seismic design technical brief No. 11
MacRae G, Kimura Y, Roeder C (2004) Effect of column stiffness on braced frame seismic behavior. J Struct Eng ASCE 130:381–391
Manson SS (1954) Behavior of materials under conditions of thermal stress. National Advisory Commission on Aeronautics, Report 1170. Lewis Flight Propulsion Laboratory, Cleveland
McCormick J, Aburano H, Ikenaga M, Nakashima M (2008) Permissible residual deformation levels for building structures considering both safety and human elements. In: Proceedings of the 14th world conference on earthquake engineering, pp 12–17
OpenSEES (2007) Open system for earthquake engineering simulation. Pacific Earthquake Engineering Research Center, Berkeley
Pandikkadavath M, Sahoo DR (2016) Analytical investigation on cyclic response of buckling-restrained braces with short yielding core segments. Int J Steel Struct 16:1273–1285
Piedrafita D, Maimí P, Cahis X (2015) a constitutive model for a novel modular all-steel buckling restrained brace. Eng Struct 100:326–331
Qin X, Zhen Z, Shao-Ping M (2020) Experimental investigation of the hysteretic performance of self-centering buckling-restrained braces with friction fuses. Eng Struct 203:109865
Razavi SA, Mirghaderi SR, Hosseini A (2014) Experimental and numerical developing of reduced length buckling-restrained braces. Eng Struct 77:143–160
Sabelli R, Mahin S, Chang C (2003) Seismic demands on steel braced frame buildings with buckling-restrained braces. Eng Struct 25:655–666
Saeki E (1997) Hysteresis characteristics of steels and buckling restrained unbonded braces. Doctoral Thesis, Tokyo Institute of Technology
Seismosoft, SeismoMatch (2016) A computer program for spectrum matching of earthquake records. https://www.seismosoft.com
Tong J, Gou Y, Pan W, Shen M, Zhou P (2020) Global buckling prevention of reduced-core-length buckling-restrained braces: theoretical and numerical investigations. Bull Earthq Eng 18:1777–1804

Tremblay R, Bolduc P, Neville R, Devall R (2006) Seismic testing and performance of buckling-restrained bracing systems. Can J Civ Eng 33:183–198

Uriz P (2005) Towards earthquake resistant design of concentrically braced steel structures. Doctoral dissertation. Berkeley: Structural Engineering, Mechanics, and Materials, Department of Civil and Environmental Engineering, University of California

Wada A, Connor J, Kawai H, Iwata M, Watanabe A (1992) Damage tolerant structure. In: 5th US-Japan workshop on the improvement of building structural design and construction practices

Wang H, Nie X, Pan P (2017) Development of a self-centering buckling restrained brace using cross-anchored pre-stressed steel strands. J Constr Steel Res 138:621–632

Watanabe A, Hitomi Y, Saeki E, Wada A, Fujimoto M (1988) Properties of brace encased in buckling-restraining concrete and steel tube. In: Proceedings ninth world conference on earthquake engineering, pp 719–724

Yamamoto M, Sone T (2014) Damping systems that are effective over a wide range of displacement amplitudes using metallic yielding component and viscoelastic damper in series. Earthq Eng Struct Dyn 43:2097–2114

Zaruma S, Fahnestock LA (2018) Assessment of design parameters influencing seismic collapse performance of buckling restrained braced frames. Soil Dyn Earthq Eng 113:35–46

Zub CI, Stratan A, Dubina D (2019) Modelling the cyclic response of structural steel for FEM analyses. ITM Web Conf 29:02011

Publisher's Note Springer Nature remains neutral with regard to jurisdictional claims in published maps and institutional affiliations.